Liquid film evaporation inside an inclined channel: Effect of the presence of a porous layer

Amine Terzi, Walid Foudhil, Souad Harmand, Sadok Ben Jabrallah

International Journal of Thermal Sciences 109 (2016) 136-147

Liquid film evaporation inside an inclined channel: Effect of the presence of a porous layer

A. Terzi [a, b, *], W. Foudhil [a], S. Harmand [c], S. Ben Jabrallah [a, b]

[a] Laboratoire d'Energétique et des Transferts Thermique et Massique, Faculté des Sciences de Tunis, Campus Universitaire, 1060 Tunis, Université El Manar, Tunisia

[b] Faculté des Sciences de Bizerte, 7021, Bizerte, Université de Carthage, Tunisia

[c] Université de Lille Nord de France, F-59000 Lille UVHC/TEMPO, F-59313 Valenciennes Cedex, France

Keywords:
Evaporation
Porous layer
Liquid film
Heat and mass transfer

A b s t r a c t

In this paper, we numerically investigate the improvement of the heat and mass transfer during the evaporation of a liquid film by introducing a liquid saturated porous layer inside an inclined channel. To achieve this, we solved the non linear partial differential equations that describe the physical system using the finite volume method in both phases (liquid saturated porous layer and gas). Compared to the liquid case, the use of the porous layer promotes the heat and mass transfer. This improvement is greater when we increase the air inlet velocity and we decrease the porosity and the thickness of the porous medium. We also propose correlations that allows us to relate the Nusselt and Sherwood numbers to the Reynolds and Biot numbers.

1. Introduction

The phenomena of heat and mass transfer during the flow of a liquid film on a heated wall has a considerable interest in the engineering field, which was translated into many applications, such as in desalination, distillation, drying, and the cooling of electronic components. In order to understand the heat and mass transfer better, different geometries were studied. Firstly, the flow of a liquid was examined on a horizontal flat plate [1]. We cite Siow et al. [2], who studied the evaporation of a laminar model within a horizontal channel. Yuan et al. [3] conducted a study on the coupled transfer of heat and mass from a thin film of water subjected to a flow of moist air.

Thereafter, several studies addressed the case of a vertical plate in order to improve the flow of the liquid. Ben Jabrallah et al. [4] studied the coupled heat and mass transfer in a rectangular cavity that acts as a distillation cell. Cherif et al. [5] experimentally studied the natural and forced convection evaporation of a thin liquid film that flows on the inner faces of the plates of a vertical channel. Fahem et al. [6] numerically analyzed the heat and mass transfer within a distillation cell. Debbissi et al. [7] studied the evaporation of water by free and mixed convection into humid air and superheated steam. Jingchun and Yicm [8] conducted a theoretical study to analyze the transient evaporation characteristics of a water film attaching to an adiabatic solid wall.

Later on, other researchers have studied evaporation on an inclined plane [9–11], which affects gravitational forces and decreases the rate of fluid flow. We cite Zeghmati and Daguenet [12] who realised a study of transient laminar free convection over an inclined wet flat plate. Agunaoun and Daif [13] studied the evaporation of a thin film of water flowing on an inclined plane surface at a constant temperature that is higher than the air temperature.

From the discussions above, it is clear that researchers have studied different geometries and conducted parametric studies on almost all input parameters that may influence the heat and mass transfers.

On the other hand, alternative solutions, such as the use of binary fluids, have also been proposed to improve transfer. Cherif and Daif [14] numerically studied the heat and mass transfer between two vertical flat plates in the presence of a binary liquid film that flows on one heated plate. Debbissi et al. [15] studied the evaporation of a binary liquid film in a vertical channel.

However, obtaining a homogenous liquid film over the entire

* Corresponding author. Laboratoire d'Energétique et des Transferts Thermique et Massique, Faculté des Sciences de Tunis, Campus Universitaire, 1060 Tunis, Université El Manar, Tunisia.

E-mail address: terziamine@hotmail.fr (A. Terzi).

DOI : 10.1016/j.ijthermalsci.2016.05.018

Nomenclature

Bi	Biot number [−]
c	mass fraction [−]
C	inertia coefficient [−]
C_p	heat capacity at constant pressure [J Kg^{-1} K^{-1}]
d	thickness of porous layer [m]
D	mass diffusivity [m^2 s^{-1}]
Da	Darcy number [−]
Fr	Froude number [−]
g	gravity acceleration [m s^{-2}]
H	channel width [m]
h	heat transfer coefficient [W m^{-2} K^{-1}]
k	thermal conductivity of the fluid [W m^{-1} K^{-1}]
K	permeability [m^2]
L	length of the channel [m]
Le	Lewis number [−]
L_v	latent heat of water [J Kg^{-1}]
m_{ev}	evaporated flow rate [Kg s^{-1} m^{-2}]
Nu_L	Latent Nusselt number [−]
p	pressure [Pa]
P^*	dimensionless pressure [−]
Pr	Prandlt number [−]
Re_g	Reynolds number [−]
Sc	Schmidt number [−]
Sh	Sherwood number [−]
T	Temperature [K]
u,v	velocity components [m s^{-1}]
U,V	dimensionless velocity components [−]
W	dimensionless mass fraction [−]
(x,y)	cartesian coordinates [m]
(X,Y)	dimensionless cartesian coordinates

Greek symbols

θ	dimensionless temperature [−]
ε	porosity [−]
μ	dynamic viscosity [Pa s]
ν	kinematic viscosity [m^2 s^{-1}]
ν^*	kinematic viscosity ratio of liquid to air [−]
ρ	density [Kg m^{-3}]
α	thermal diffusivity [m^2 s^{-1}]
δ	dimensionless thickness of porous layer [−]
φ	relative humidity at inlet [−]
ϕ	inclined angle [−]
τ	dimensionless inertia coefficient of porous medium [−]

Subscripts

l	liquid phase
g	gas phase
e	effective
i	liquid gas interface
s	solid
w	wall

plate constitutes a major discrepancy between the theoretical and experimental studies. Despite efforts in the field of modeling and numerical simulation, we still see a difference between calculation and experiment. In a previous work, Cherif et al. [16], have studied the two aspects of evaporation film: experiment and simulation. A difference was reported. They believe that this difference is caused by the difficulty of making a falling film on a vertical plate. In fact, the film cannot be controlled if it is directly adhered to the plate. To analyze the effect of dry zones on the plate, Mammou et al. [17] numerically studied the evaporation along an inclined plate. This plate consists of two wet zones separated by dry zone. The results of this study showed that the length of the dry zone plays an important role.

More recent studies have explored various techniques to solve this problem. For example, several researchers utilized rough surfaces, or interposed obstacles [18]. For example, Zheng and Worek [19] numerically and experimentally studied the evaporation of a liquid film inside an inclined channel. They fixed glass rods on the plate to disrupt the flow of liquid, thus improving the heat and mass transfer.

We believe that the best way to achieve a falling film on a flat plate and control its characteristics is the application of a porous layer that serves as a support for the liquid film. Few studies have theoretically examined the effect of the presence of a porous medium during evaporation [20,21]. Part of the reason for this is that the coupled heat and mass transfer process in the presence of such medium becomes more complicated.

As a result, this work focuses on the study of the evaporation of a saturated porous layer inside an inclined airflow channel. The main objective of this study is to evaluate the effect of introducing a liquid saturated porous layer on the heat and mass transfer. Specifically, this study examines the influence of parameters such as the air inlet velocity and the structural properties of the porous material (thickness, porosity), on the performance of the evaporation. We also propose correlations that allows as to define the Nusselt and Sherwood numbers based on the Reynolds and Biot numbers.

2. Mathematical formulation

We studied the evaporation of a liquid film in an inclined channel that consisted of two flat plates separated by a distance H. The liquid flows onto the plate from below, which is maintained at a constant temperature T_w and covered with a porous layer of thickness d. The second plate is adiabatic. A laminar descending flow of humid air flowed through the channel. At the entrance, the temperature of the gas was $T_{0g} = T_{0\ l} = T_{amb}$, the humidity was φ_0 and the velocity was uniform at V_0 (Fig. 1).

To simplify the problem, we will consider the following assumptions [22]:

- The liquid and gas flows are laminar, stationary and two-dimensional.
- There is no slip between the liquid and gas flows.
- Moist air is an ideal mixture of water vapor and dry air, which is considered an ideal gas.
- The effect of surface tension is negligible.
- The liquid-vapor interface is free of waves, in local thermodynamic equilibrium and impermeable to air-drying.
- The mass transfer induced by heat diffusion (Soret effect) and the heat transfer induced by a concentration gradient (Dufour effect) are negligible.

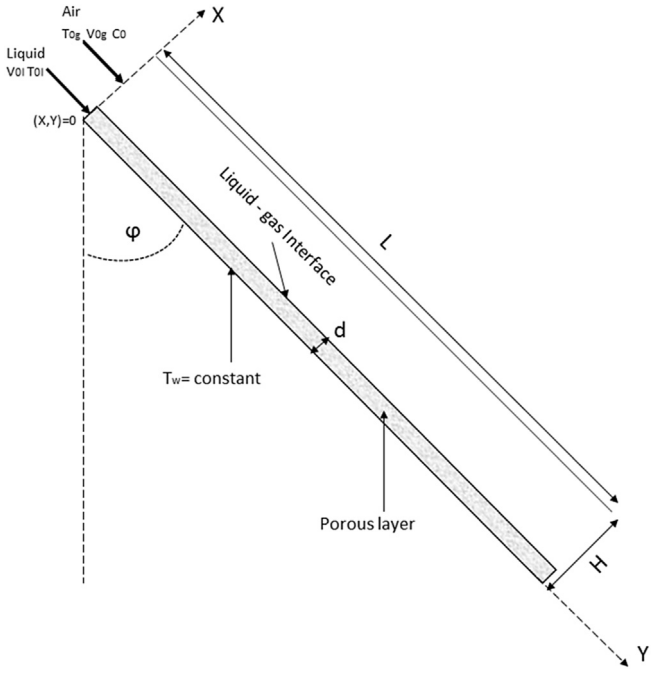

Fig. 1. Schematic presentation of the physical domain.

- Radiation in the fluid, viscous dissipation and pressure work are neglected in the energy balance equation.
- Local thermal equilibrium is assumed in the porous medium.

2.1. Governing equations

2.1.1. In the porous layer

The stationary equations describing the flow and the transfer in the liquid saturated porous layer are based on the local volume averaging technique [23]. They include the continuity equation, the energy equation and the Darcy-Brinkman-Forchheimer equation.

continuity equation

$$\frac{\partial u}{\partial x}+\frac{\partial v}{\partial y}=0 \tag{1}$$

u and v momentum equations

$$\rho_l g sin\phi-\frac{\mu_l}{K}u+\frac{\mu_l}{\varepsilon}\left(\frac{\partial^2 u}{\partial y^2}+\frac{\partial^2 u}{\partial x^2}\right)-\frac{\rho_l C u^2}{\sqrt{K}}=0 \tag{2}$$

$$\rho_l g cos\phi-\frac{\mu_l}{K}v+\frac{\mu_l}{\varepsilon}\left(\frac{\partial^2 v}{\partial y^2}+\frac{\partial^2 v}{\partial x^2}\right)-\frac{\rho_l C v^2}{\sqrt{K}}=0 \tag{3}$$

The permeability K, is expressed in terms of the porosity ε and the particle diameter. It is defined as follows [24]:

$$K=\frac{d^2\varepsilon^3}{150(1-\varepsilon)^2}$$

energy equation

$$u\frac{\partial T}{\partial x}+v\frac{\partial T}{\partial y}=\alpha_e\left(\frac{\partial^2 T}{\partial x^2}+\frac{\partial^2 T}{\partial y^2}\right) \tag{4}$$

The effective thermal diffusivity α_e is expressed in terms of the effective thermal conductivity k_e. The two parameters are defined as follows [25,26]: $\alpha_e = k_e/\rho_l c_{p,l}$ with $k_e = \varepsilon k_l + (1-\varepsilon)k_s$

2.1.2. In the gas phase

In the gas phase, we consider the continuity equation, momentum equation, energy equation and species conservation equation, described in the steady state.

continuity equation

$$\frac{\partial u}{\partial x}+\frac{\partial v}{\partial y}=0 \tag{5}$$

u and v momentum equations

$$\rho u\frac{\partial u}{\partial x}+\rho v\frac{\partial u}{\partial y}=-\frac{\partial p}{\partial x}+\mu\left(\frac{\partial^2 u}{\partial x^2}+\frac{\partial^2 u}{\partial y^2}\right) \tag{6}$$

$$\rho u\frac{\partial v}{\partial x}+\rho v\frac{\partial v}{\partial y}=-\frac{\partial p}{\partial y}+\mu\left(\frac{\partial^2 v}{\partial x^2}+\frac{\partial^2 v}{\partial y^2}\right) \tag{7}$$

energy equation

$$u\frac{\partial T}{\partial x}+v\frac{\partial T}{\partial y}=\alpha_g\left(\frac{\partial^2 T}{\partial x^2}+\frac{\partial^2 T}{\partial y^2}\right) \tag{8}$$

Species conservation equation

$$u\frac{\partial c}{\partial x}+v\frac{\partial c}{\partial y}=D\left(\frac{\partial^2 c}{\partial x^2}+\frac{\partial^2 c}{\partial y^2}\right) \tag{9}$$

2.1.3. Boundary conditions

The boundary conditions associated to this problem, are given as fellow.

- At the inlet, the liquid has the following characteristics:

$$\text{at } y=0,: \qquad T_l=T_{0l}, \quad u_l=u_{0l}, \quad v_l=v_{0l} \tag{10}$$

T_{0l}, u_{0l} and v_{0l} are respectively the temperature and the velocity values at the inlet of the liquid domain.

- For the gas phase,

$$\text{at } y=0,: \qquad T_g=T_{0g}, \quad u_g=u_{0g}, \quad v_g=v_{0g}, \quad c=c_0 \tag{11}$$

T_{0g}, u_{0g} and v_{0g} are respectively the temperature and the velocity values at the inlet of the gas phase. c_0 represents the concentration value at the inlet of the gas domain.

- At the walls,

$$\text{at } x=0,: \qquad T=T_w, \quad u=0, \quad v=0 \tag{12}$$

$$\text{at } x=H,: \qquad u=0, \quad v=0, \quad \frac{\partial T}{\partial x}=0, \quad \frac{\partial c}{\partial x}=0 \tag{13}$$

- At the liquid air interface, for the u component of the velocity

$$u_i = u_{l,i} = u_{g,i} \tag{14}$$

the transverse interface velocity is given by the following:

$$u = \frac{-D}{(1-c)_i}\left(\frac{\partial c}{\partial x}\right)_i \tag{15}$$

for the v component of the velocity,

$$v_i = v_{l,i} = v_{g,i} \tag{16}$$

$$\mu_l\left(\frac{\partial v_l}{\partial x}\right)_i = \mu_g\left(\frac{\partial v_g}{\partial x}\right)_i \tag{17}$$

for the temperature,

$$T_i = T_{l,i} = T_{g,i} \tag{18}$$

Assuming thermodynamic equilibrium is established and the vapor-air mixture is a perfect gas, the continuity of the heat flux is given by the following:

$$-k_e\left(\frac{\partial T}{\partial x}\right)_i = -k_g\left(\frac{\partial T}{\partial x}\right)_i + m_{ev}L_v \tag{19}$$

m_{ev} is the evaporated flow rate, and it is calculated as following:

$$m_{ev} = \frac{-\rho_g D}{(1-c)_i}\left(\frac{\partial c}{\partial x}\right)_i \tag{20}$$

2.2. Modeling under dimensionless form

To derive the dimensionless numbers that describe the problem, the equations of conservations should be recast in dimensionless form. To this end, we adopt the following change of variables:

$$X = \frac{x}{H}, Y = \frac{y}{H}, \delta = \frac{d}{H}, U = \frac{u}{v_{0g}}, V = \frac{v}{v_{0g}}, \theta = \frac{T-T_0}{T_w-T_0}, W = \frac{c-c_0}{c_i-c_0}, P^* = \frac{p-p_0}{\rho_g v_{0g}^2} \tag{21}$$

2.2.1. In the porous layer

Given the dimensionless variables adopted, all the variables in the previous equations in the porous domain (1)–(4) take the following form:

continuity equation

$$\frac{\partial U}{\partial X} + \frac{\partial V}{\partial Y} = 0 \tag{22}$$

u and v momentum equation

$$\frac{Re_g\delta^2}{\nu^* Fr^2} - \frac{1}{Da}U + \frac{\delta^2}{\varepsilon}\left(\frac{\partial^2 U}{\partial X^2} + \frac{\partial^2 U}{\partial Y^2}\right) - \frac{\tau U^2}{Da} = 0 \tag{23}$$

$$\frac{Re_g\delta^2}{\nu^* Fr^2} - \frac{1}{Da}U + \frac{\delta^2}{\varepsilon}\left(\frac{\partial^2 U}{\partial X^2} + \frac{\partial^2 U}{\partial Y^2}\right) - \frac{\tau U^2}{Da} = 0 \tag{24}$$

energy equation

$$U\frac{\partial\theta}{\partial X} + V\frac{\partial\theta}{\partial Y} = \frac{\nu^*}{Pr_e Re_g}\left(\frac{\partial^2\theta}{\partial X^2} + \frac{\partial^2\theta}{\partial Y^2}\right) \tag{25}$$

2.2.2. In the gas phase

Given the dimensionless variables adopted, all the variables in the previous equations in the gas phase (5)–(9) take the following form:

continuity equation

$$\frac{\partial U}{\partial X} + \frac{\partial V}{\partial Y} = 0 \tag{26}$$

u and v momentum equation

$$U\frac{\partial U}{\partial X} + V\frac{\partial U}{\partial Y} = -\frac{\partial P^*}{\partial X} + \frac{1}{Re_g}\left(\frac{\partial^2 U}{\partial X^2} + \frac{\partial^2 U}{\partial Y^2}\right) \tag{27}$$

$$U\frac{\partial V}{\partial X} + V\frac{\partial V}{\partial Y} = -\frac{\partial P^*}{\partial Y} + \frac{1}{Re_g}\left(\frac{\partial^2 V}{\partial X^2} + \frac{\partial^2 V}{\partial Y^2}\right) \tag{28}$$

energy equation

$$U\frac{\partial\theta}{\partial X} + V\frac{\partial\theta}{\partial Y} = \frac{1}{Re_g Pr_g}\left(\frac{\partial^2\theta}{\partial X^2} + \frac{\partial^2\theta}{\partial Y^2}\right) \tag{29}$$

species conservation equation

$$U\frac{\partial W}{\partial X} + V\frac{\partial W}{\partial Y} = \frac{1}{Re_g Pr_g Le}\left(\frac{\partial^2 W}{\partial X^2} + \frac{\partial^2 W}{\partial Y^2}\right) \tag{30}$$

2.2.3. Dimensionless boundary conditions

The corresponding dimensionless boundary conditions are given by the following:

- At the inlet, the liquid has the following characteristics:

$$\text{at } Y = 0,: \qquad \theta_l = \theta_{0l}, \quad U_l = U_{0l}, \quad V_l = V_{0l} \tag{31}$$

- For the gas phase,

$$\text{at } Y = 0,: \qquad \theta_g = \theta_{0g}, \quad U_g = U_{0g}, \quad V_g = V_{0g} \tag{32}$$

- at the walls,

$$\text{at } X = 0,: \qquad \theta = 1, \quad U = 0, \quad V = 0 \tag{33}$$

$$\text{at } X = 1,: \qquad U = 0, \quad V = 0, \quad \frac{\partial\theta}{\partial X} = 0, \quad \frac{\partial W}{\partial X} = 0 \tag{34}$$

- at the liquid air interface,

for the U component of the velocity

$$U_i = U_{l,i} = U_{g,i} \tag{35}$$

$$U = \frac{-(c_i - c_0)}{Re_g Sc(1-c)_i}\left(\frac{\partial W}{\partial X}\right)_i \tag{36}$$

for the V component of the velocity,

$$V_i = V_{l,i} = V_{g,i} \tag{37}$$

$$\left(\frac{\partial V_l}{\partial X}\right)_i = \frac{\rho_g}{\nu^* \rho_l}\left(\frac{\partial V_g}{\partial X}\right)_i \tag{38}$$

for the temperature,

$$\theta_i = \theta_{l,i} = \theta_{g,i} \tag{39}$$

$$\left(\frac{\partial \theta}{\partial X}\right)_i = \frac{k_g}{k_e}\left(\frac{\partial \theta}{\partial X}\right)_i + \frac{\rho_g D L_v (c_i - c_0)}{k_e (1-c)_i (T_w - T_0)}\left(\frac{\partial W}{\partial X}\right)_i \tag{40}$$

2.2.4. Dimensionless number

The dimensionless numbers defined in Equations (22)–(40) are defined by:

$$Re_g = \frac{\rho_g v_{0g} H}{\mu_g}, \quad Pr_e = \frac{\nu_L}{\alpha_e}, \quad Fr = \frac{v_{0g}}{\sqrt{g cos\phi H}}, \quad Pr_g = \frac{\nu_g}{\alpha_e}, \quad Le = \frac{\alpha_e}{D}, \quad Sc = LePr_g \tag{41}$$

where Re_g, Pr, Fr, Le and Sc are Reynolds, Prandlt, Froude, Lewis and Schmidt numbers respectively.

To generalize our results, we characterized the heat and mass transfer at the liquid gas interface using the dimensionless Nusselt and Sherwood numbers. We adopted expressions similar to those used by W.M.Yan [27], who studied the evaporation of a falling film on a heated vertical air channel under airflow with a second adiabatic plate:

$$Nu_L(y) = \frac{m_{ev}(y) L_v H}{k_g (T_i(y) - T(H,y))} \tag{42}$$

$$Sh(y) = \frac{m_{ev}(y) H (1 - c_i(y))}{\rho_g D (c_i(y) - c(H,y))} \tag{43}$$

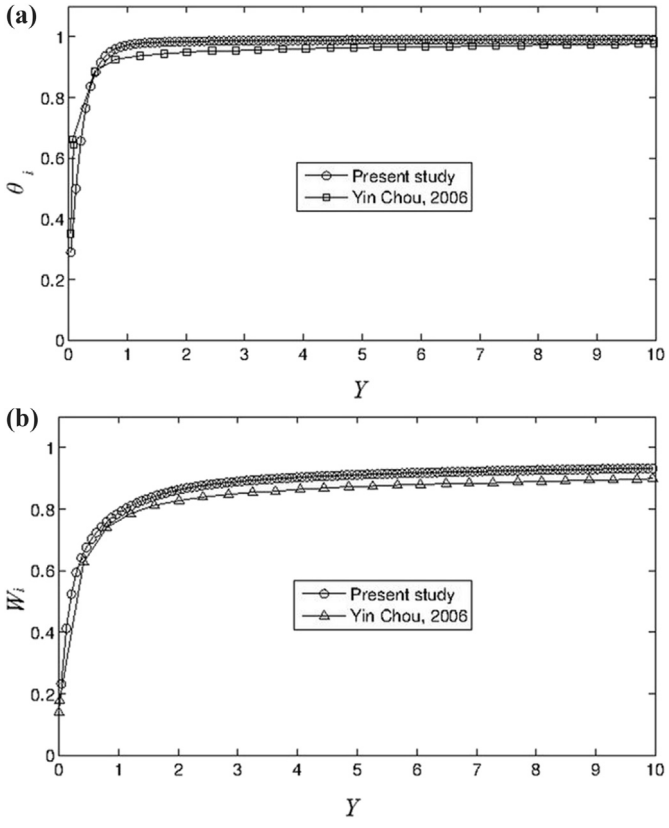

Fig. 2. Comparison of our results with those published by Yin Chou [21]: Variation of the dimensionless temperature (a) and the dimensionless concentration (b) at the liquid gas interface according to the dimensionless length ($Re_g = 500$, $\varepsilon = 0.4$, $\delta = 0.2$).

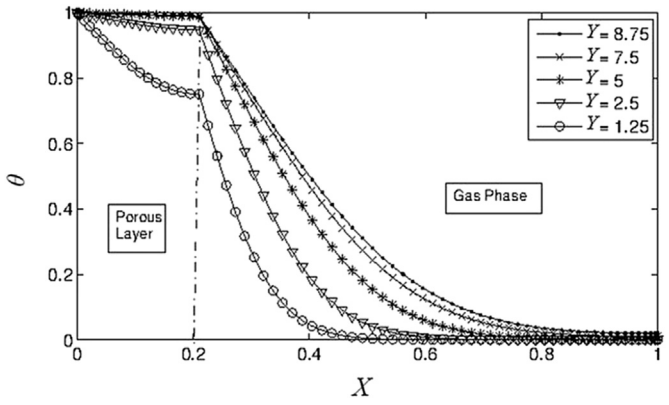

Fig. 3. Evolution of the dimensionless temperature in both phases for different sections of the channel ($Re_g = 500$, $\varepsilon = 0.8$, $\delta = 0.2$).

3. Numerical method

The non linear partial differential equations that describe the problem were solved numerically using the finite volume method [28,29]. The grid is non uniform in both directions, expanding far from the boundaries, using a large number of meshes in the neighborhood of the wall, at the inlet and outlet of the domain. The mesh in the liquid porous layer was finer than the mesh in the gas domain. The term coupling velocity and pressure is solved by the algorithm **SIMPLE** [29] and a power law schema is adopted to define the convective and diffusive terms in the partial differential equations.

Our code was validated for the evaporation of a liquid film

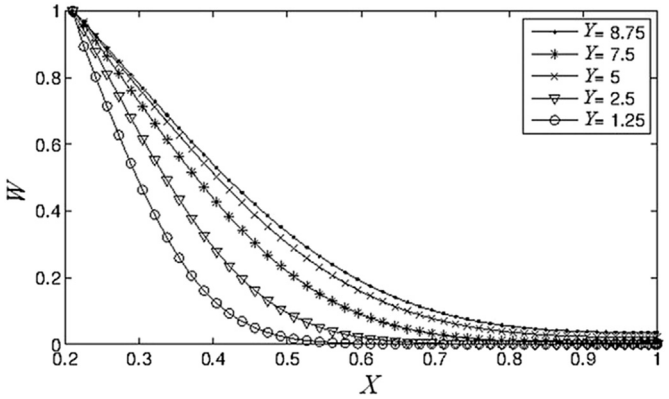

Fig. 4. Evolution of the dimensionless concentration in the gas phase for different sections of the channel ($Re_g = 500$, $\varepsilon = 0.8$, $\delta = 0.2$).

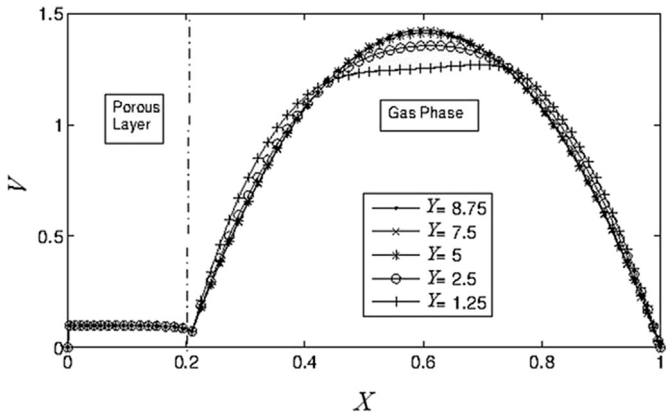

Fig. 5. Evolution of the dimensionless velocity in both phases for different sections of the channel ($Re_g = 500$, $\varepsilon = 0.8$, $\delta = 0.2$).

flowing on the lower wall of a vertical channel covered with a porous layer. We compared our results to those found in the literature by Yin Chou [21] for an imposed constant temperature $T = T_w$ at the wet plate. The other plate is thermally insulated. This comparison concerned a flow of water with an inlet temperature of T_0 equal to that of the inlet gas. The spacing between the plates is H. We performed a comparison with the results giving the variations of the temperature and the concentration at the liquid gas interface. Fig. 2 shows good agreement between our results and those of Yin Chou [21], as the relative difference is less than 3%.

4. Results and discussion

In this section, we present the results of the simulation. These results are classified according to five components. We first describe the thermal and dynamic fields within the channel, in both liquid and gas phases. Thereafter, we present results showing the effect of introducing the porous layer. This part will be followed by a parametric study to examine the effect of the characteristics of the porous layer. We provide summary tables and we finish the work by the proposal of some correlations.

4.1. Distribution of the temperature, the concentration and the velocity inside the channel

Fig. 3 describes the cross-sectional variation of the temperature in both phases (liquid and gas). This description is made at several heights of the channel. In the gaseous medium, the curves show intense heat exchange near the liquid gas interface. Beyond half the length of the channel ($X = 0.6$), this exchange is substantially reduced. To better understand this phenomenon, we present the cross-sectional variations of the concentration at different heights of the channel in Fig. 4. Intense mass transfer was observed in the same area ($0.2 < X < 0.6$), which in turn consumes all of the energy. We also note that these profiles are comparable to the temperature in the gas phase. This similarity can be explained by the analogy between the energy Equation (8) and the species conservation Equation (9).

Fig. 5 shows the evolution of the dimensionless longitudinal velocity as a function of the dimensionless cross sections of the

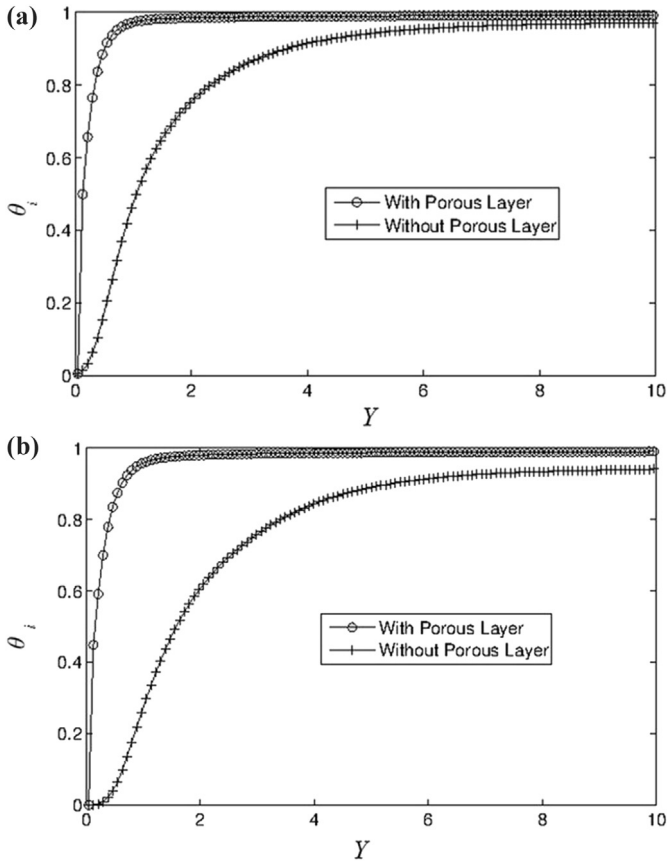

Fig. 6. Effect of introducing a liquid saturated porous layer on the variation of the dimensionless interfacial temperature according to the dimensionless length (a. $Re_g = 500$) (b. $Re_g = 900$).

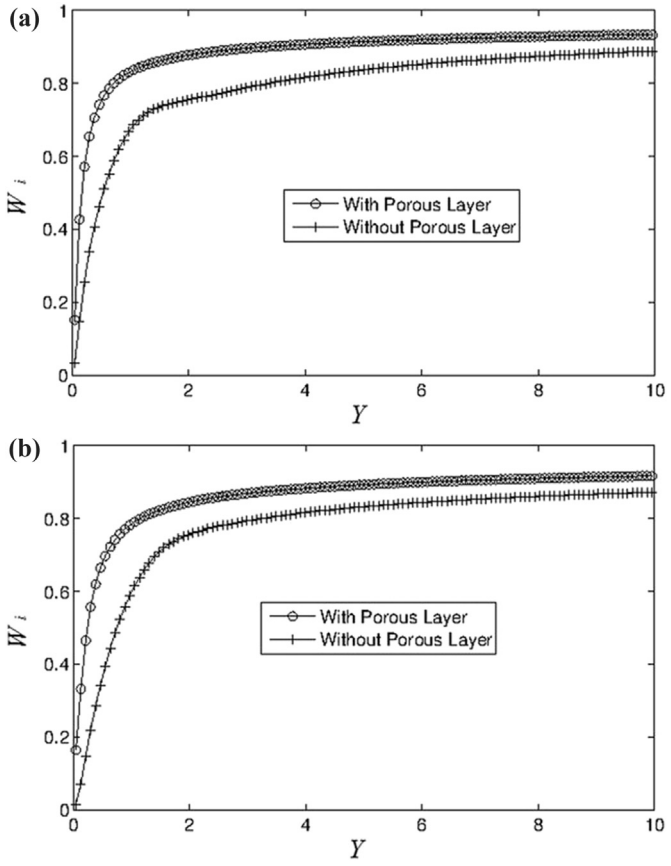

Fig. 7. Effect of introducing a liquid saturated porous layer on the variation of the dimensionless interfacial concentration according to the dimensionless length (a. $Re_g = 500$) (b. $Re_g = 900$).

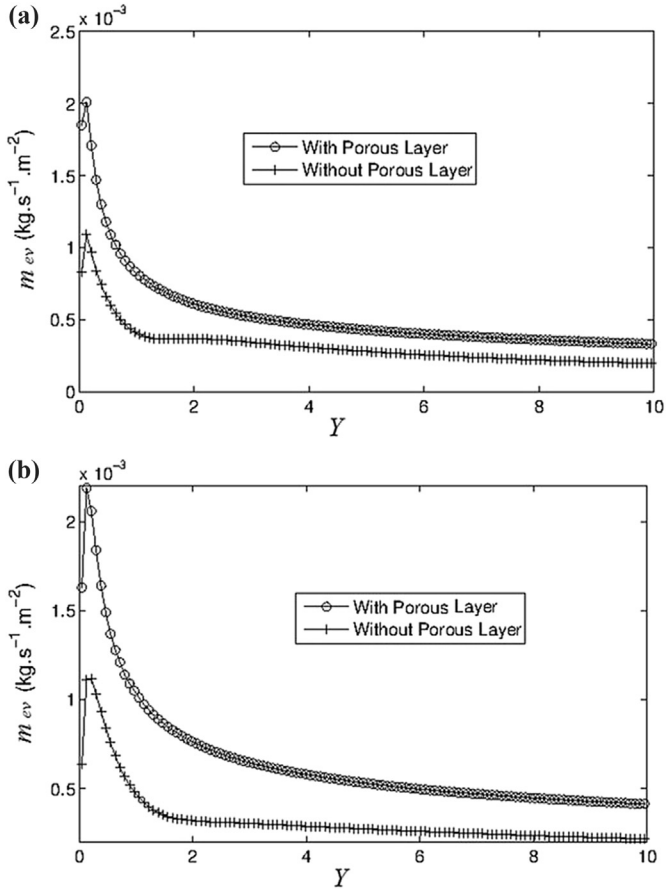

Fig. 8. Effect of introducing a liquid saturated porous layer on the variation of the evaporated flow rate at the liquid-gas interface according to the dimensionless length (a. $Re_g = 500$) (b. $Re_g = 900$).

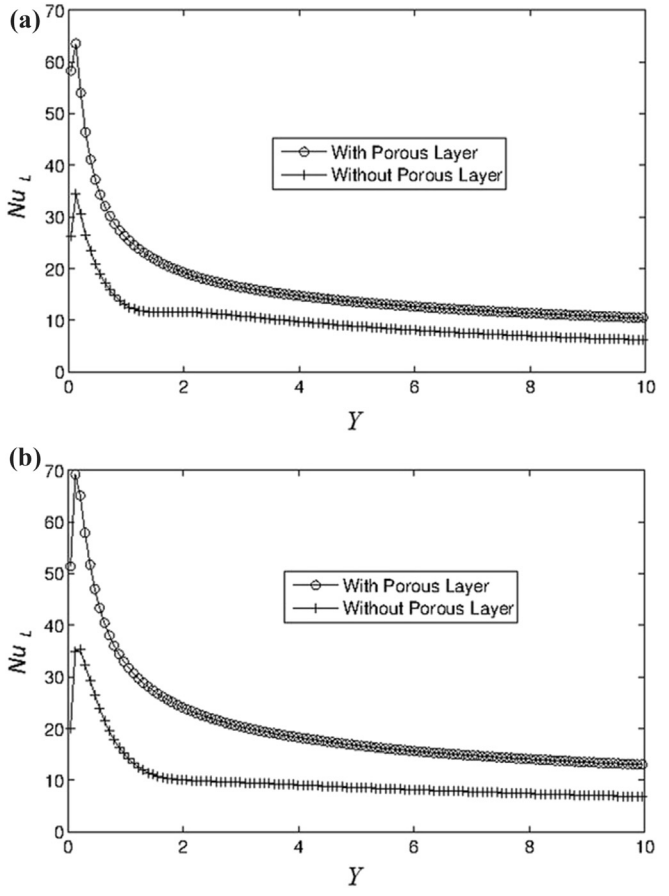

Fig. 9. Effect of introducing a liquid saturated porous layer on the variation of the latent Nusselt number at the liquid-gas interface according to the dimensionless length (a. $Re_g = 500$) (b. $Re_g = 900$).

channel distance. The velocity profile in the gas phase tends to be symmetric and parabolic. The vapor creation velocity has been taken into account. However, its effect on the dynamic field in the gas phase is not visible because its value is relatively small compared with the velocity of the gas. In addition, the interface behaves as a rigid flat wall, which is in agreement with the results of A. Agunaoun [13]. In the liquid, due to the low inlet flow and the low permeability of the porous layer, the longitudinal velocity varies slightly with the calculation position. This result validates the often-used assumption that the liquid velocity receives a slight variation according to the height.

4.2. Effect of the porous layer

In this section, we study the effect of introducing a liquid saturated porous materiel on the heat and mass exchange. For this, we represent in Fig. 6 the variation of the temperature at the liquid gas interface for both configurations with and without a porous layer. The results are shown for two Reynolds numbers. Observing the curves of Fig. 6, we find that the temperature at the liquid-gas interface is higher in the presence of the porous medium. The effect of this increase in temperature affects the mass exchange. We present in Fig. 7 the evolution of the concentration at the liquid gas interface for the two configurations with and without a porous layer. As for the interfacial temperature, concentrations are higher in the presence of the porous layer. We conclude that introducing a liquid saturated porous material also improves the mass exchange. This result is in agreement with the results illustrated in Fig. 8. In fact in this figure we present the evolution of the evaporated flow rate for both configurations with and without porous medium, which increases when we use the porous layer.

Figs. 9 and 10 describe the variation of the latent Nusselt number Nu_L and Sherwood number Sh at the liquid-gas interface, respectively. In this zone, the general shape of these figures is similar to that of the evaporation flow rate (Fig. 8). Moreover, the Equations (46) and (47) defined above show that the Nu_L and Sh values depend on m_{ev}.

4.3. Parametric study

After comparing the two configurations with and without porous layer, to ensure the efficacy of introducing a liquid saturated porous materiel on the heat and mass exchange, it is interesting to find the best configuration to use.

In the following, we will study the effect of the porosity of the Reynolds number and the thickness of the porous layer.

Fig. 11 illustrates the variation of the dimensionless temperature as a function of the length for different Reynolds numbers and different porosity at the liquid-gas interface. It is found that the value of the temperature reduces as the Reynolds number

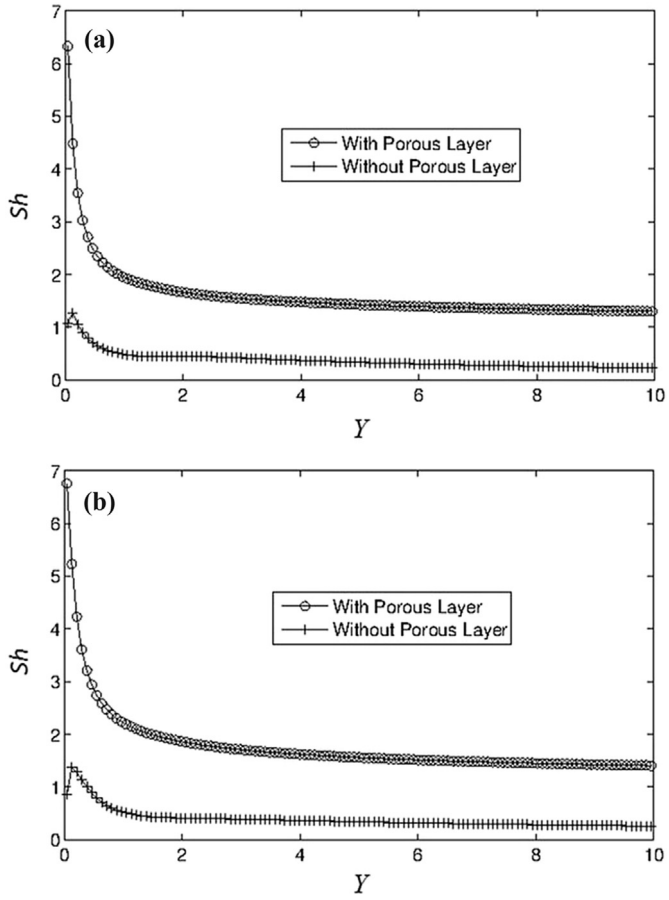

Fig. 10. Effect of introducing a liquid saturated porous layer on the variation of the Sherwood number at the liquid-gas interface according to the dimensionless length (a. $Re_g = 500$) (b. $Re_g = 900$).

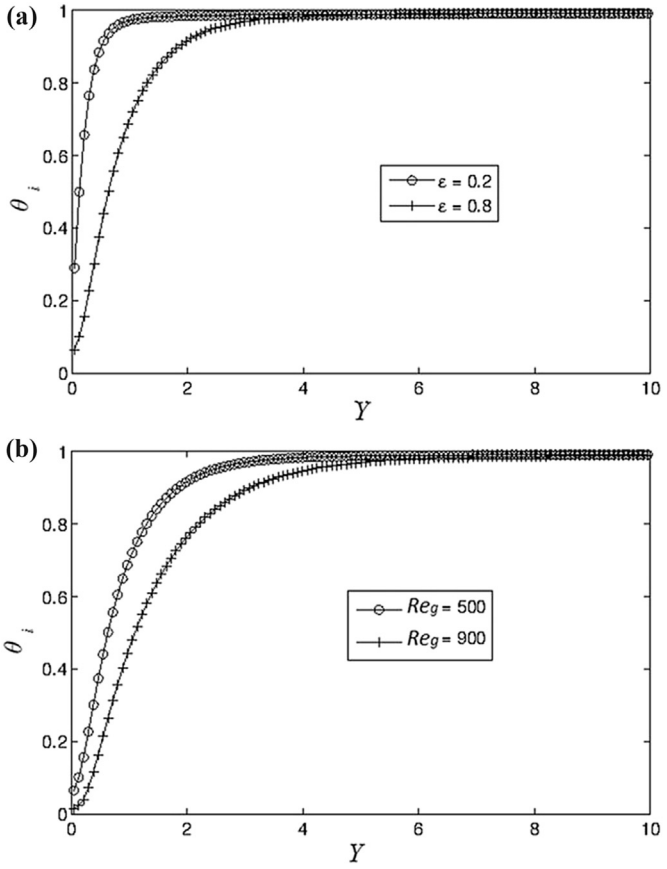

Fig. 11. Evolution of the dimensionless interfacial temperature according to the dimensionless length (a. $Re_g = 500$) (b. $\varepsilon = 0.8$).

increases, which confirms the general concept that the heat transfer is more important with higher Reynolds numbers. We also note that the interfacial temperature decreases as the porosity increases. The reason for this is that a decrease in the porosity ameliorates the effective conductivity and therefore improves heat transfer.

Fig. 12 shows the variation of the dimensionless concentration according to the length for different Reynolds numbers and different porosity at the liquid gas interface. The shapes of the profiles are the same as that of the temperature profile (Fig. 11). As for the temperature, it is observed that the concentration increases with reducing Reynolds number and porosity.

Fig. 13 shows the variation of the dimensionless longitudinal velocity as a function of the transverse distance in the middle of the channel for different porosity. In the liquid phase, the velocity decreases with reducing porosity. Indeed, increasing the porosity increases the permeability of the porous medium, which allows the liquid to permeate faster. In the gas phase, we note that the decrease in porosity creates an acceleration of the air flow in the channel. Indeed, as we have already mentioned, the decrease in porosity improves evaporation. The air becomes more saturated with vapor which has a lower density than dry air.

Fig. 14 shows the evaporated flow variation throughout the liquid gas interface for different porosity and Reynolds numbers. The evaporated flow is improved with the increase of the Reynolds number which is in agreement with the general concept that the mass transfer is enhanced in airstream with higher Reynolds numbers. The results also show that the evaporated flow is improved with reducing the porosity. This implies that the addition of the porous layer ameliorate the mass transfer. The reason for this is that the porous layer increases the heat transfer area of the liquid film.

Figs. 15 and 16 describe the variation of the latent Nusselt number Nu_L and Sherwood number Sh at the liquid-gas interface, respectively. Similar to the evaporation flow, the latent Nusselt number and the Sherwood number increases with the increase of the Reynolds number and reducing the porosity.

Fig. 17 show the variation of the Nusselt and Sherwood numbers for different thicknesses of the porous layers. The evaporated flow is important for small values of d. A thick porous layer decreases the interfacial temperature and thus reduces the heat and mass transfer.

4.4. Tables of results comparison

In this section, tables gather the values of the mean Nusselt numbers, the evaporated flow rate and the Sherwood numbers with respect to Reynolds number and porosity. From the results of Table 1, we find that for a fixed Reynolds number (Re = 500) the film with low porosity ($\varepsilon = 0.2$) presents an amelioration of the evaporated flow rate of 40%. This improvement decreases for a

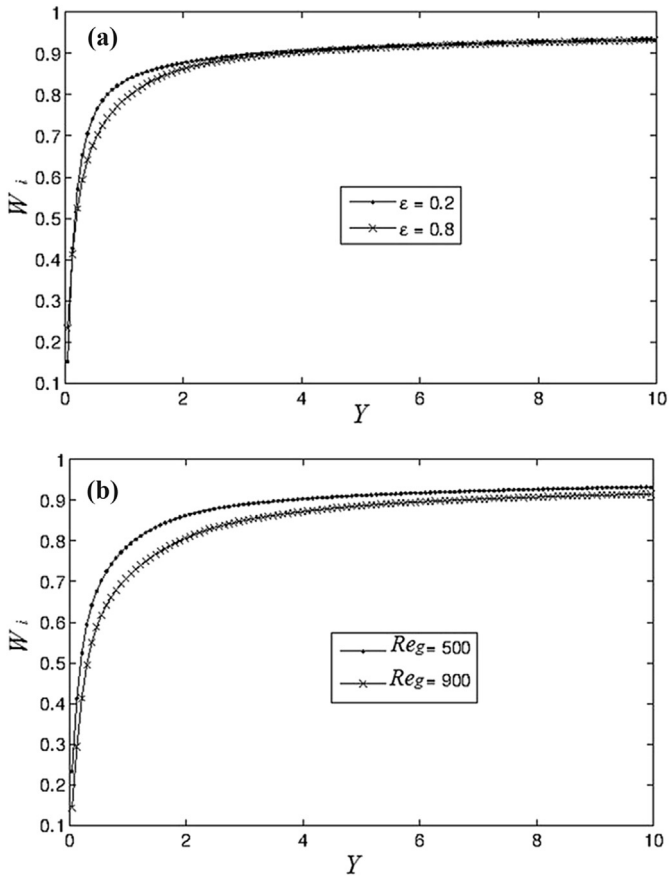

Fig. 12. Evolution of the dimensionless interfacial concentration according to the dimensionless length (a. $Re_g = 500$) (b. $\varepsilon = 0.8$).

porosity $\varepsilon = 0.8$. Indeed, for this value, the porous medium approaches a fluid medium. On the other hand, and by fixing the porosity, we notice an improvement of the evaporated flow rate when we increase the velocity of the air flow (Reynolds number). To highlight the role of the porous layer in improving the heat transfer in the liquid gas interface, we grouped in Table 2 the values of

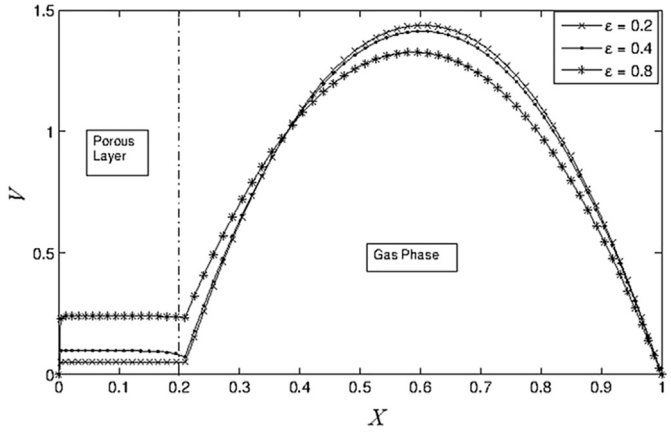

Fig. 13. Evolution of the dimensionless velocity in both phases in the middle of the channel: Influence of porosity ($Re_g = 500$, $\delta = 0.2$).

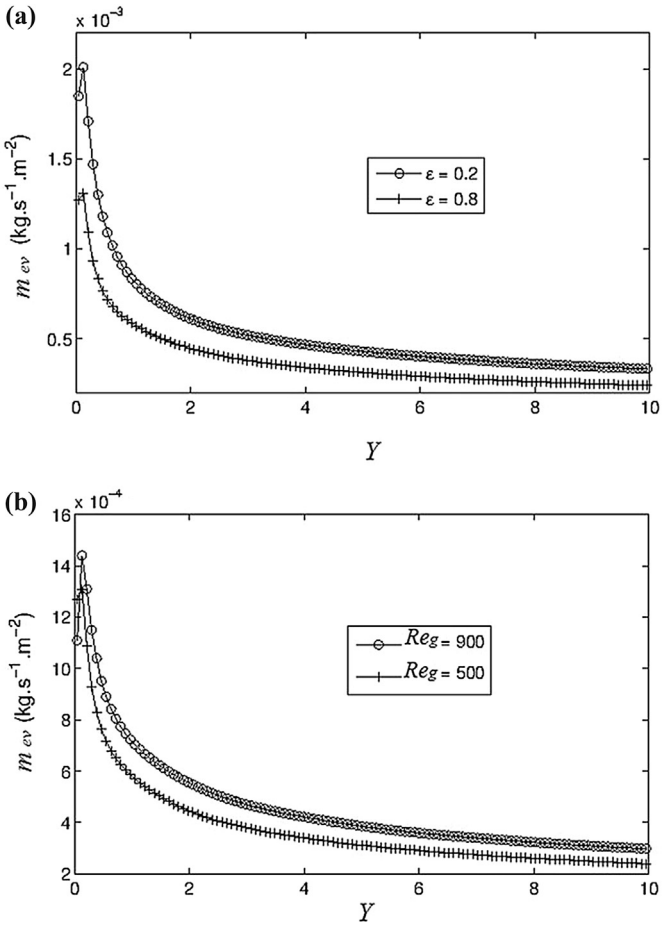

Fig. 14. Variation of the evaporated flow rate at the liquid-gas interface according to the dimensionless length (a. $Re_g = 500$) (b. $\varepsilon = 0.8$).

Nusselt and Sherwood numbers for both configurations without and with the porous medium in place for both different porosity and Reynolds number. The values provided in Table 2 confirm those in Table 1.

4.5. Correlation

We represent in Figs. 18 and 19 the variations of the Nusselt and Sherwood numbers as a function of the Reynolds number for different Biot numbers, respectively. The values of the Reynolds number are situated in the interval [100, 1000]. As a result, we attempted to identify correlations that allow us to define each of these variables (Nusselt number and Sherwood number) based on the Reynolds number and the Biot number:

$$Nu_L = 0.2198 Re^{0.3498} Bi^{-0.2494} \quad (44)$$

$$Sh = 0.0535 Re^{0.1795} Bi^{-0.2627} \quad (45)$$

where the Biot number is expressed us follows:

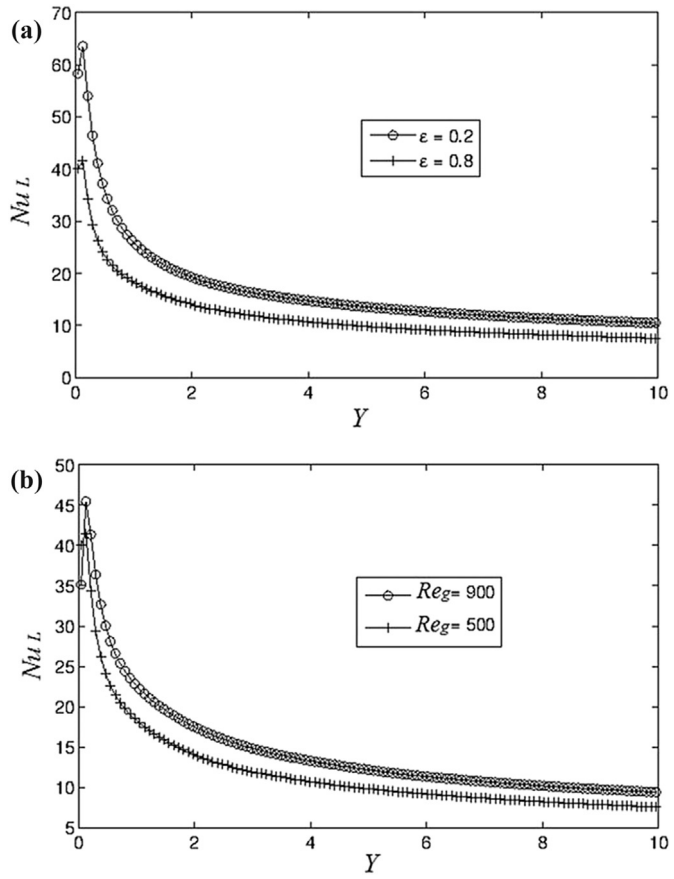

Fig. 15. Variation of the latent Nusselt number at the liquid gas interface according to the dimensionless length (a. $Re_g = 500$) (b. $\varepsilon = 0.8$).

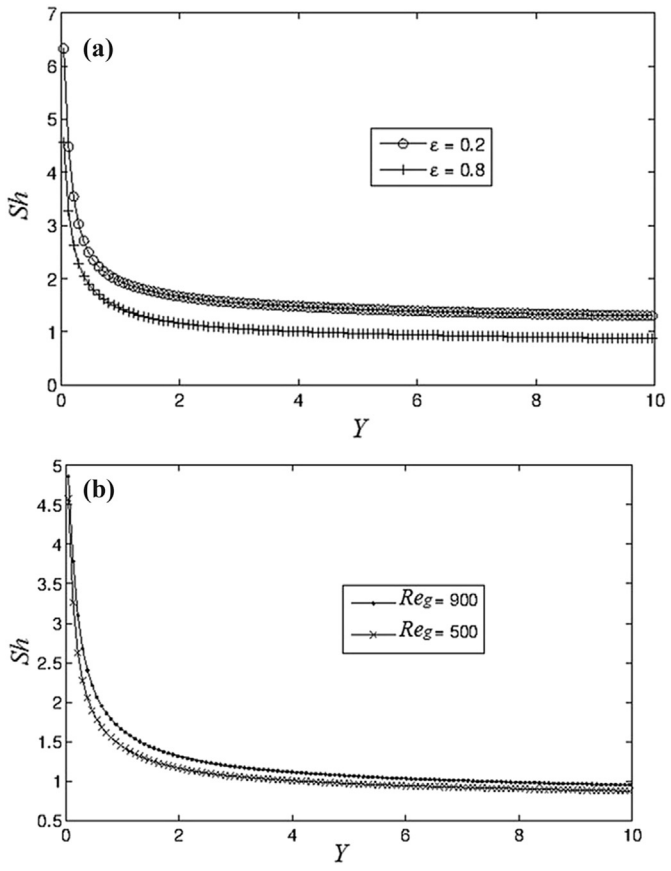

Fig. 16. Variation of the Sherwood number at the liquid gas interface according to the dimensionless length (a. $Re_g = 500$) (b. $\varepsilon = 0.8$).

$$Bi = \frac{hd}{k_e} \tag{46}$$

and h is the heat transfer coefficient:

$$h = -\frac{k_g(\partial T/\partial y)_i}{T_i - T_0} \tag{47}$$

The choice of a correlation type $F = aRe^bBi^c$, is made for two main reasons. Firstly, in the literature, to our connaissance, this type of correlation has not been proposed in the case of the evaporation of a liquid film in the presence of a porous medium for an inclined plane. Secondly, the use of the Reynolds and Biot numbers includes all parameters that can influence the variation of the Nusselt and Sherwood numbers and therefore the heat and mass transfer in the channel.

4.6. Conclusion

This work is aimed at the analysis of the influence of introducing a liquid saturated porous medium on the heat and mass transfer during the evaporation of a liquid film in an inclined channel. We begin this study by describing the distribution of the temperature, concentration and velocity in both phases (liquid saturated porous layer and gas). Then we performed a comparison between the two configurations (with and without porous medium) to highlight the effect of its addition. We find that introducing the porous layer improves heat and mass exchanges in the channel. More specifically, and from the performed parametric study, we conclude that

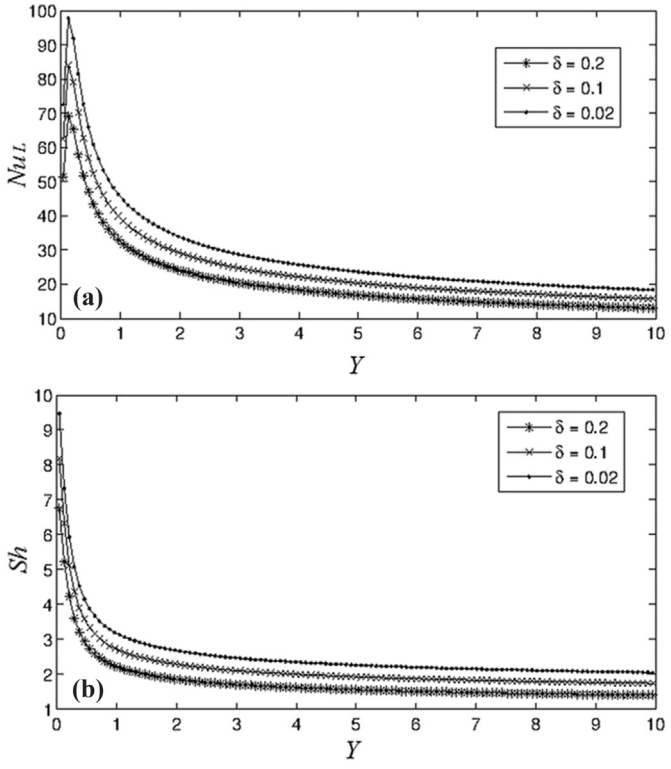

Fig. 17. Variation of the Nusselt and Sherwood numbers at the liquid gas interface according to the dimensionless length for different thickness of the porous layer (a. $Re_g = 900$) (b. $\varepsilon = 0.2$).

Table 1
Amelioration of the average evaporated flow rate with introducing a liquid saturated porous layer (effect of the porosity and Reynolds number).

Re_g	Without porous layer	With porous layer		%
$Re_g = 500$	$M_{ev}(Kg{\cdot}s^{-1}) = 3.19{\cdot}10^{-4}$	$\varepsilon = 0.2$	$M_{ev}(Kg{\cdot}s^{-1}) = 5.33{\cdot}10^{-4}$	40.15
		$\varepsilon = 0.8$	$M_{ev}(Kg{\cdot}s^{-1}) = 3.78{\cdot}10^{-4}$	15.6
$Re_g = 900$	$M_{ev}(Kg{\cdot}s^{-1}) = 3.24{\cdot}10^{-4}$	$\varepsilon = 0.2$	$M_{ev}(Kg{\cdot}s^{-1}) = 6.55{\cdot}10^{-4}$	50.53
		$\varepsilon = 0.8$	$M_{ev}(Kg{\cdot}s^{-1}) = 4.64{\cdot}10^{-4}$	30.17

Table 2
Amelioration of the average Nusselt and Sherwood numbers with introducing a liquid saturated porous layer (effect of the porosity and Reynolds number).

Re_g	Without porous layer	With porous layer		%
$Re_g = 500$	$Nu_L = 10.06$	$\varepsilon = 0.2$	$Nu_L = 16.83$	40.22
		$\varepsilon = 0.8$	$Nu_L = 11.94$	15.74
	$Sh = 0.37$	$\varepsilon = 0.2$	$Sh = 1.6$	76
		$\varepsilon = 0.8$	$Sh = 1.11$	66
$Re_g = 900$	$Nu_L = 10.22$	$\varepsilon = 0.2$	$Nu_L = 20.67$	50.55
		$\varepsilon = 0.8$	$Nu_L = 14.63$	30.14
	$Sh = 0.39$	$\varepsilon = 0.2$	$Sh = 1.78$	78
		$\varepsilon = 0.8$	$Sh = 1.24$	68

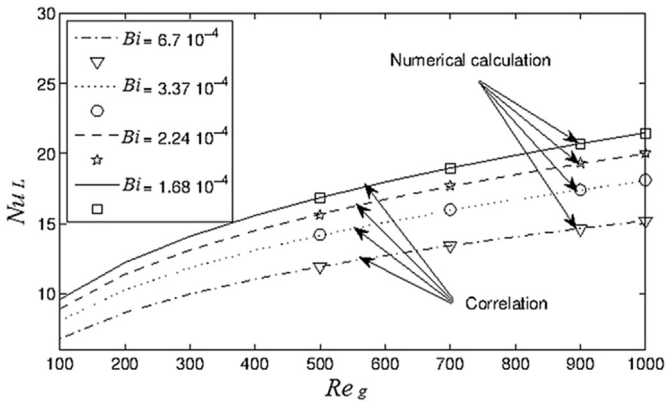

Fig. 18. Nusselt number variation as a function of the Reynolds number for different Biot numbers.

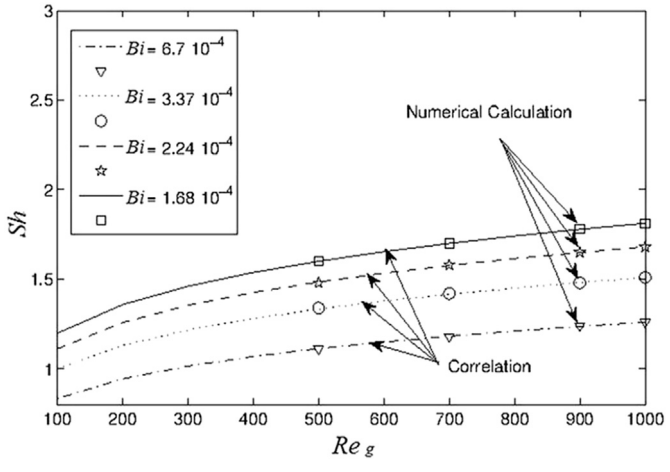

Fig. 19. Sherwood number variation as a function of the Reynolds number for different Biot numbers.

the use of the porous medium is more efficient for high Reynolds numbers, low porosity and low thickness. Finally, we present the variation of the Nusselt and Sherwood numbers describing the heat and mass exchanges within the channel depending on the Reynolds and Biot numbers.

References

[1] Raimundo AM, Gaspar AR, Virgilio A, Divo MO, Quintela A. Wind tunnel measurements and numerical simulations of water evaporation in forced convection airflow. Int J Therm Sci 2014;86:28–40.
[2] Siow EC, Ormiston SJ, Soliman HM. Fully coupled solution of a two-phase model for laminar film condensation of vapor gas mixtures in horizontal channels. Int J Heat Mass Transf 2002;45:3689–702.
[3] Yuan ZX, Yan XT, Ma CF. A study of coupled convective heat and mass transfer from thin water film to moist air flow. Int Commun Heat Mass Transf 2004;31:291–301.
[4] Jabrallah S Ben, Belghith A, Corriou JP. Convective heat and mass transfer with evaporation of a falling film in a cavity. Int. J. Therm. Sci. 2005;45:16–28.
[5] Cherif AS, Jabrallah S Ben, Corriou JP, Belghith A. Intensification of the liquid film evaporation in a vertical channel. Desalination 2010;250:433–7.
[6] Fahem K, Jabrallah S Ben, Belghith A, Corriou JP. Numerical simulation of the behaviour of a distillation cell with influence of the characteristics of the heating wall. Desalination 2006;201:185–97.
[7] Debbissi C, Orfi J, Nasrallah S Ben. Evaporation of water by free or mixed convection into humid air and superheated steam. Int. J. Heat Mass Transf. 2003;46:4703–15.
[8] Min J, Tang Y. Theoretical analysis of water film evaporation characteristics on an adiabatic solid wall. Refrigeration 2015;53:55–61.
[9] Jang J, Yan W, Huang C. Mixed convection heat transfer enhancement through film evaporation in inclined square ducts. Int. J. Heat Mass Transf. 2005;48:2117–25.
[10] Yan W. Effects of film evaporation on laminar mixed convection heat and mass transfer in a vertical channel. Int. J. Heat Mass Transf. 1995;38:1261–9.
[11] Aybar HS. Evaporation model of an inclined solar water distillation system. Desalination 2006;190:63–70.
[12] Zeghmati B, Daguenet M. Study of transient laminar free convection over an inclined wet flat plate. Int. J. Heat Mass Transf. 1991;34:899–909.
[13] Agunaoun A, Daif A. Evaporation en convection forcée d'un film mince s'écoulant en régime permanent, laminaire et sans onde, sur une surface plane inclinée. Int. J. Heat Mass Transf. 1994;18:2947–56.
[14] Cherif AA, Daif A. Etude numérique du transfert de chaleur et de masse entre deux plaques planes verticales en presence d'un film de liquide binaire ruisselant sur l'une des plaques chauffée. Int. J. Heat Mass Transf. 1999;42:2399–418.
[15] Hfaiedh C Debbissi, Nasr A, Nasrallah S Ben. Evaporation of a binary liquid film flowing down the wall of two vertical plates. Int. J. Therm. Sci. 2013;72:34–46.
[16] Cherif AS, Kassim MA, Benhamou B, Harmand S, Corriou JP, Jabrallah S Ben. Experimental and numerical study of mixed convection heat and mass transfer in a vertical channel with film evaporation. Int. J. Therm. Sci. 2011;50:942–53.
[17] Hfaiedh CDebbissi, Nasr A, Nasrallah S Ben. Numerical study of heat and mass transfer from an inclined flat plate with wet and dry zones. Int. J. Heat Mass Transf. 1992;35:2277–87.
[18] Gonda A, Lancereau P, Bondelier P, Luo L, Fan Y, Benezech S. Water falling film evaporation on a corrugated plate. Int. J. Therm. Sci. 2014;81:29–37.
[19] Zheng GS, Worek WM. Method of heat and mass transfer enhancement in film evaporation. Int. J. Heat Mass Transf. 1996;39:97–108.
[20] Leu J, Jang J, Chou Y. Heat and mass transfer for liquid film evaporation along a vertical plate covered with a thin porous layer. Int. J. Heat Mass Transf. 2006;49:1937–45.
[21] Chou Y, Yang R. The evaporation of a saturated porous layer inside an inclined airflow channel. Int. J. Heat Mass Transf. 2007;28:407–17.
[22] Jabrallah S Ben, Belghith A, Corriou JP. Study of heat and mass transfer in a rectangular cavity: application to a distillation cell. Int. J. Heat Mass Transf. 2002;45:891–904.
[23] Whitaker S. Simultaneous heat, mass, and momentum transfer in porous media: a theory of drying. Adv. Heat Transf. 1977;13:119–203.
[24] Ergun S. Fluid flow through packed columns. Chem. Eng. Prog. 1952;48:89–94.

[25] Alazmi B, Vafai K. Analysis of fluid flow and heat transfer interfacial conditions between a porous medium and a fluid layer. Int. J. Heat Mass Transf. 2001;44:1735–49.
[26] Alazmi B, Vafai K. Analysis of variants with the porous media transport models. J. Heat Transf. 2000;122:303–26.
[27] Yan WM. Effects of film evaporation on laminar mixed convection heat and mass transfer in a vertical channel. Int. J. Heat Mass Transf. 1992;35:3419–29.
[28] Patankar S, Spalding D. A calculation procedure for heat, mass and momentum transfer in three dimensional parabolic flow. Int. J. Heat Mass Transf. 1972;15:1781–806.
[29] Patankar SV. Numerical Heat Transfer and Fluids Flow. Hemisphere; 1980.